Report on RUNE's coastal experiment and first inter-comparisons between measurements systems

Floors, Rogier Ralph; Lea, Guillaume; Pena Diaz, Alfredo; Karagali, Ioanna; Ahsbahs, Tobias Torben

Publication date:
2016

Document Version
Publisher's PDF, also known as Version of record

Report on RUNE's coastal experiment and first inter-comparisons between measurements systems

DTU Wind Energy E-Report

Rogier Floors, Guillaume Lea, Alfredo Peña, Ioanna Karagali, Tobias Torben Ahsbahs

DTU Wind Energy-E-Report-0115 (EN)
August 2016

DTU Wind Energy
Department of Wind Energy

Author: Rogier Floors, Guillaume Lea, Alfredo Peña, Ioanna Karagali, Tobias Torben Ahsbahs
Title: Report on RUNE's coastal experiment and first inter-comparisons between measurement systems
Department: DTU Wind Energy

DTU Wind Energy E-0115
November 11, 2016

ISBN:
978-87-93278-72-1

Abstract (max. 2000 char)

Accurate description of the wind energy resource in the coastal zone is crucial for countries developing near-shore wind farms. The RUNE experiment aims to use lidar measurements and mesoscale modelling to study the behaviour of the flow in the coastal zone and find the most effective way to estimate the near-shore wind resource. In this report we document all information regarding the measurement systems and the coastal campaign.

The wind speed is estimated from radial velocities measured by a lidar in sector-scanning mode, from two lidars performing dual-overlapping scans and from five vertical profiling lidars, of which one was operating offshore on a floating platform. All these instruments are inter compared, showing generally good agreement. The availability is best for the vertically profiling lidars, followed by the sector-scan setup, the dual setup and the lidar buoy. We have also reference measurements from the meteorological mast at Høvsøre some kilometers south of the campaign's site.

The wind climate during the campaign is characterized by strong westerlies with occasional storms. The measurements from the vertically profiling lidars agree well with those from the meteorological mast and show a decrease of mean wind speed from west to east. Two lidars (a long- and a short-range system) measuring next to each other measured similar winds speeds, although the wind speed from the long-range lidar had a small positive bias. There was also a positive bias in the mean wind speed from the sector-scan at large measuring distances.

Satellite winds from ASCAT, Sentinel-1 and TerraSAR-X were available. ASCAT were of coarse resolution and were not used for any direct comparisons with the lidar measurements. A spatial average of these SAR wind speeds along the coast was compared with coinciding scanning lidar 10 min wind speeds.

TerraSAR-X retrieved winds showed a rather large deviation from the lidar wind speed transects extrapolated to 10 m. Sensitivity tests performed on the methods for the wind speed retrieval showed small differences in the statistics for the different combinations of the spatial resolution and the polarisation ratio. For the cases investigated, the wind direction from the model was not differing by more than 15° compared to the dual setup, but the spatial variability was not captured.

Sponsorship:
The ForskEL programme, project nr. 12263 "RUNE"

Pages: 33
Tables: 5
Figures: 21
References: 25

Technical University of Denmark
Frederiksborgvej 399
4000 Roskilde
Denmark
Tel. +4546775024
rofl@dtu.dk
www.vindenergi.dk

Contents

1 Introduction

The wind resource in areas near the coastline is difficult to predict due to the large changes in surface roughness, topography and land-sea interactions (Floors et al., 2013; Vincent et al., 2013). The RUNE experiment was designed to gauge the uncertainty of measured and modelled wind speeds in this area and explore new ways of measuring the wind speed offshore from land-based locations.

For wind resource estimation near the coast, models such as WAsP (Wind Atlas Analysis and Application Program) can be used, but also mesoscale models are becoming increasingly popular (Frank et al., 2001; Landberg et al., 2003; Nunalee and Basu, 2014). One of these is the Weather Research and Forecasting (WRF) model, which has been combined with a microscale model to provide detailed wind resource estimations (Badger et al., 2014). This method relies on 'generalization' of the model output, which is then downscaled using the WAsP methodology. Near the coast this method has a higher uncertainty, due to large differences in surface roughness and thermal properties of land and sea. These modelling issues will be addressed in a separate report and in this paper we focus only on the measurements.

The uncertainty in wind resource estimations can be brought down significantly by using measurements at the site of interest. Traditionally, these are performed with a meteorological mast, but these are often expensive to install and have a long lead time. Wind lidars in vertically profiling mode have been commercially available for several years and are generally accepted as tools to determine the wind resource (Gottschall et al., 2012). More recently, scanning lidars with a steerable scanning head have also appeared on the market, which provide new ways to determine the long-term mean wind resource.

One of these scanning lidar systems is the Windscanner system: it can be used to map the wind over a predetermined scanning pattern (Vasiljević, 2014; Berg et al., 2015). The system can measure the flow field by emitting the laser beams from two or more spatially separated lidars, directing them to intersect, and moving the beam intersection over an area of interest. To save costs, also a single lidar can be used to scan a certain part of the atmosphere and determine the wind speed components (assuming some characteristics of the scanned volume).

Recently, also lidars mounted on buoys became available. Such a device will be deployed and can be used to evaluate the scanning lidar at a far offshore position. Finally, the use of satellite products can give additional insights on the spatial structure of the offshore wind field. These products can also be evaluated well with the spatial wind fields obtained from a scanning lidar.

Combining all these measurements provides a unique dataset for evaluations of the coastal flow and the goal of this report is to provide all necessary information about the measuring systems that have been deployed during the campaign and the campaign itself. In Sect. 2 we present the devices and in Sect. 3 we give the locations and describe the terrain where they were installed. In Sect. 4 the time line of the deployment is given, together with details about the configuration settings, scanning patterns and the available satellite data. In Sect. 5 we present the wind climate, how the filtering of the measurements affected the availability, inter-compare the wind speeds available from all data sources. Finally we conclude and summarise this report in Sect. 6.

2 Instruments

The RUNE experiment used lidars with a fixed and steerable scanner head. All scanning lidars are part of the Windscanner infrastructure from the Technical University of Denmark (DTU) Wind Energy (Vasiljević, 2014). They are based on the commercial WindCube WLS200S from Leosphere operating with a laser with a wavelength of 1.54 μm. Throughout this document we will use the names from Table 1 to refer to the individual lidars. The lidars Sterenn and Koshava were used in a time-synchronized manner and detailed technical information about a similar coordinated system of long-range WindScanners is given in Berg et al. (2015).

The vertically profiling lidars were mostly Doppler systems 'WindCube WLS7' from Leosphere. Alizé is a Leosphere WindCube WLS70, i.e. a long-range Doppler system. These wind lidars have been extensively evaluated against mast measurements (Gottschall and Courtney, 2010; Floors et al., 2013; Peña et al., 2015).

				Position (UTM, WGS84, Zone 32V)		
Loc. Nr.	Name	Designation	Usage	x (m)	y (m)	z (m)
1	Koshava	WLS200S-007	Dual setup	446080.03	6259660.30	12.36
2	Vara	WLS200S-012	Sector scan	445915.64	6261837.49	26.38
2	Alizé	WLS70-001	Vertical Profile	445915.64	6261837.49	26.38
2	WLS66	WLS7-066	Vertical Profile	445915.64	6261837.49	26.38
3	Sterenn	WLS200S-006	Dual setup	445823.66	6263507.90	42.97
4	3E	WLS7-007	Vertical Profile	446379.30	6263251.46	43.18
5	Bura	WLS7-002	Vertical Profile	447040.74	6263273.41	24.93
6	Lidar Buoy Pos1	WLS7-277	Vertical Profile	438441	6262178	0.00
7	Lidar Buoy Pos2	WLS7-277	Vertical Profile	440616	6262085	0.00
8	Høvsøre mast	-	Mast	447642	6255431	0.32
9	Wave buoy	-	-	438236	6262181	0.00

Table 1. Information about the measurement systems that were operating during the campaign.

3 Site and terrain description

3.1 Description of the terrain at the experimental site

The experiment took place in a rather homogeneous, open landscape covered with large meadows and some scattered buildings and trees (Fig. 1, left). In general, the landscape is undulating and there is a drop in the terrain elevation near the sea associated with a cliff at the coastline (Fig. 2). The topography of the area at a horizontal resolution of 1.6 m can be obtained via the website of the Geostyrelsen (Geostyrelsen, 2016). Land-cover data from the CORINE dataset can be obtained via the website of the EEA (EEA, 2016). The land-use classes can be associated with an approximate surface roughness length z_0 by using Table 1 in Pindea et al. (2002).

The land-use classes around the site are shown in Fig. 1 (right). The yellow area around the site is associated with annual cropland ($z_0 = 0.2$ m). The villages of Bøvlingbjerg ($\approx$3 km east of the Høvsøre meteorological mast) and Ramme ($\approx$5 km east of the experimental site) are the most prominent features that will impact the flow from a easterly direction at the site. The build-up areas show $z_0 = 0.8$ m in the reclassified CORINE data. The mixed forest area $\approx$10 km east of the site can also have an impact on the flow at higher measuring heights in the campaign. Note that the roughness values that are discussed here are based on simple reclassification of the land-use data, but Peña et al. (2016) found that the surface roughness at Høvsøre is much lower. They found that z_0 is varying with season, direction and atmospheric stability; the all-sector long-term $z_0 = 0.012$ m. The differences between the CORINE dataset-derived roughnesses and the observed values is partly due to the applicability of the dataset; in mesoscale applications the roughnness has to be representative for a grid cell of a kilometre or more, which is often higher than the local roughness due to the non-linear impact of obstacles on the flow.

3.2 Positions of the instruments

The positions of the instruments deployed during the RUNE campaign are listed in Table 1. For all scanning lidars it was made sure that the scanning area was unobstructed (Courtney and Simon, 2016). The scanning patterns of the different devices will be described in Sect. 4.2. Vara was positioned at the coast near the cliff, on the grass next to the lavatory near a church at $\approx$26 m above mean sea level (amsl). Koshava was placed to the south in open grassland in front of a house, at a location where the cliff is not as high ($\approx$15 m amsl). Sterenn was placed to the North at one of the highest points, 20 m south of a lighthouse on an abandoned military bunker. The location of the instruments was measured using a differential GPS system with an accuracy of $\approx$10 cm. More information on the site identification for RUNE can be found in Courtney and Simon (2016).

The lidars Alizé and WLS66 were installed next to Vara. The lidar 3E was installed more inland $\approx$ 500 m west of Sterenn and North of Vara. Bura was installed east of 3E. Photographs of the locations can be found in Courtney and Simon (2016).

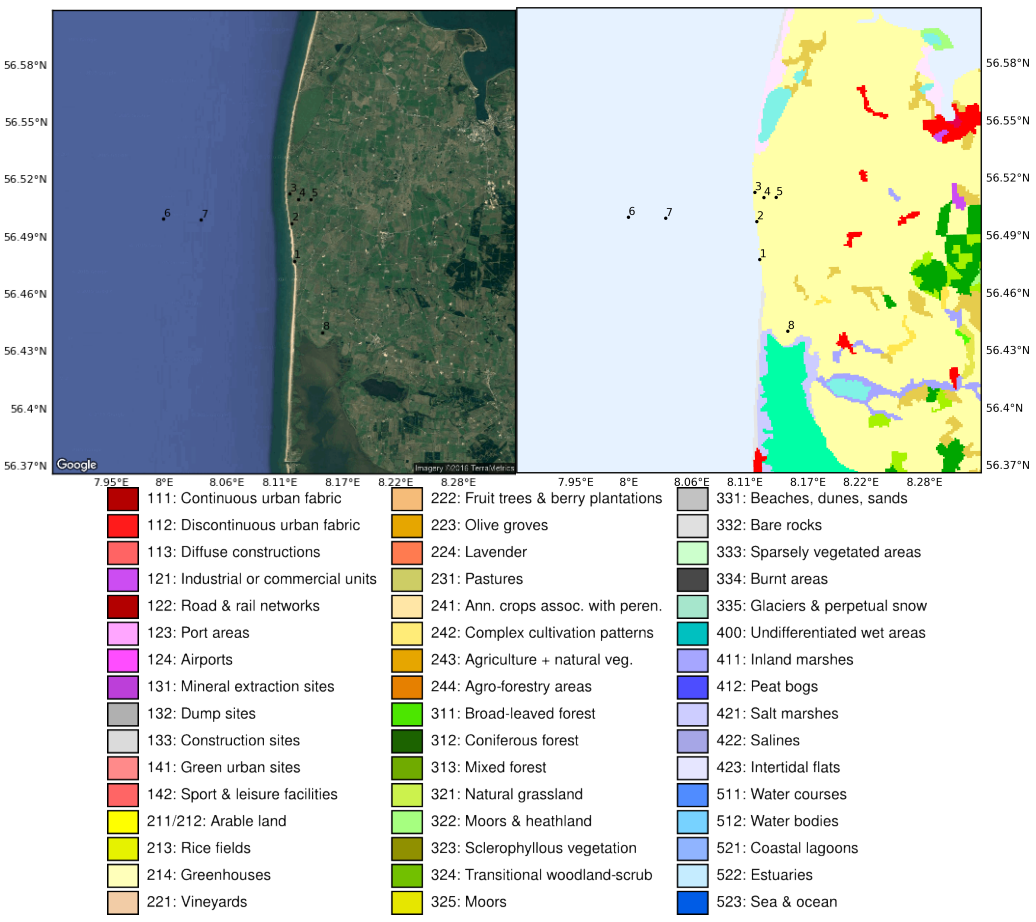

Figure 1. Satellite picture of the terrain around the site (left) and land use classes around the site. The main positions described in Sec. 4.2 are given as numbered black points.

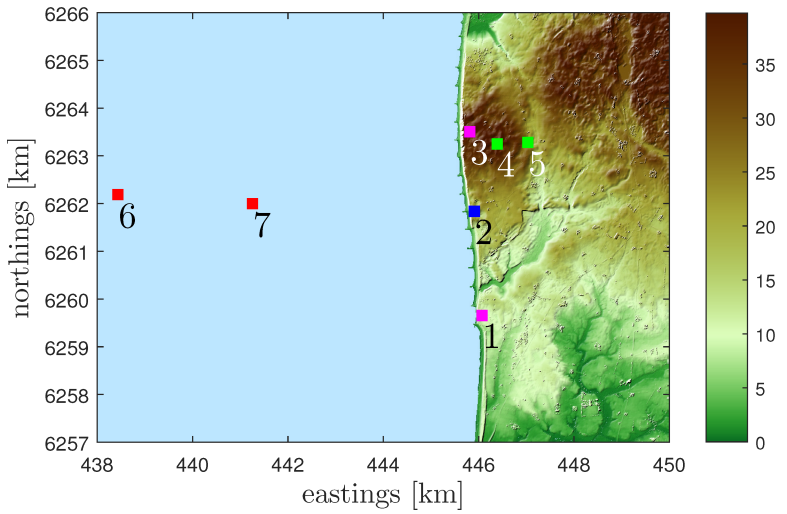

Figure 2. Topographic description (colours) of the terrain around the experimental site and the positions of the lidars denoted with numbered points (Table 1).

4 Data description

4.1 Timeline of the campaign

The RUNE campaign started at the beginning of November and lasted until the end of February. Four different phases are distinguished during the measurement campaign based on the scanning patterns of the WindScanners and described in Table 2.

4.1.1 First phase

During this phase the lidars were calibrated using fixed targets and the scanning trajectories were prepared. During alignment and trajectory coding, all three Windscanners were used in a 'sector-scan' scenario at 1 elevation angle (see Sect. 4.2.1 for details). The azimuthal angle covered by the scans was 60° facing west. Note: during this phase, the area experienced several winter storm events.

4.1.2 Second phase

This phase started on the 26th of November, when Vara was setup in a 'sector-scan' scenario at three elevation angles (Sect. 4.2.1), whereas Sterenn and Koshava followed a dual setup (Sect. 4.2.2).

4.1.3 Third phase

Taking advantage of a major hardware failure experienced by Koshava, the trajectories of Koshava and Sterenn were modified to reduce the spacial distance between range gates used for reconstruction of the wind speed. This resulted in a second database with reconstructed wind speeds at slightly different coordinates (see Appendix A).

4.1.4 Fourth phase

During the final phase, Vara was setup in a 'sector-scan' scenario covering an azimuthal angle of 120° at an elevation angle of ≈0°. The two other WindScanners were used in a synchronised dual setup to measure along a virtual mast (Sect. 4.2.3).

4.2 Instrument setup and scanning patterns

4.2.1 Sector-scan

The 'sector-scan' scenario, technically known as Plan Position Indicator (PPI), consists of one lidar scanning positions that cover several azimuths at a fixed elevation angle. During phase 2, Vara used PPI 60° scans facing west at three different elevations. These elevations were chosen such that they reach a 50, 100 and 150 m amsl at 5 km offshore. For the three scans, an IVAP (Integrated Velocity Azimuth Processing) algorithm has been used to reconstruct the horizontal wind components at each range gate. The IVAP algorithm uses a summation of the angularly separated line-of-sight (LOS) velocities (Liang, 2007).

The full trajectory was taking 145 s to complete: 45 s for each scan at the 3 different elevations and 10 s to travel back to the first measurement point. Each scan obtained 45 LOS velocities with 1 s accumulation time. Each LOS contained 156 range gates from 100 m to 8150 m, so for each full scan 468 reconstructed horizontal wind components were obtained.

The reconstruction algorithm was applied for each scan and filtered out if the average Carrier-To-Noise ratio (CNR) of 45 LOS at each range gate was below -27 dB. Then the obtained wind components were averaged over 10, 30 and 60-min periods, i.e. using 4, 12 and 24 reconstructed

velocities per averaged value, respectively. In this report we only use the 10-min mean values. These 10-min mean values have been written to a high-level database which will be used for further analysis in this report (Appendix A).

Phase	System	Start Time	End Time	Scenario Type	Data (h)	Operat. Avail.
1	Vara	13/11 10:55	26/11 16:17	PPI 1 elevation	251.5	79.25%
	Sterenn	17/11 18:06	27/11 10:34	PPI 1 elevation	215.8	92.83%
	Koshava	17/11 18:06	24/11 08:42	PPI 1 elevation	145.9	91.99%
2	Vara	26/11 16:34	17/02 08:51	PPI 3 elevations	1575.2	79.38%
	Sterenn	03/12 16:26	25/12 17:40	Sync Dual Doppler V1	193.7	36.60%
	Koshava	03/12 16:26	25/12 16:48	Sync Dual Doppler V1	193.7	36.66%
3	Sterenn	25/12 18:02	17/02 08:51	Sync Dual Doppler V2	1095.7	85.15%
	Koshava	25/12 18:02	17/02 08:51	Sync Dual Doppler V2	1056.7	82.12%
4	Vara	17/02 09:16	29/02 14:43	PPI 1 elevation	269.7	91.91%
	Sterenn	17/02 09:16	29/02 06:10	RHI for Virtual Mast	281.1	98.67%
	Kosava	17/02 09:16	29/02 14:55	RHI for Virtual Mast	290.9	99.06%
All	Alizé	09/11 11:20	29/02 15:10	DBS	2625	97.52%
	Bura	12/11 11:00	28/02 20:00	DBS	2211	85.01%
	3E	01/11 00:00	02/03 23:50	DBS	2928.7	99.22%
	WLS66	01/11 01:00	29/02 11:50	DBS	2792.7	96.61%
	Buoy Pos1	04/11 08:10	07/12 08:30	DBS	792	99.96%
	Buoy Pos2	11/02 09:00	30/03 19:30	DBS	622.7	53.61%

Table 2. Description of the measurement phases in the RUNE campaign. At each phase, operational availability is defined as the number of hours of acquired data without any CNR filtering divided by the total amount of hours that the system could have acquired data.

4.2.2 Dual setup

The two WindScanners involved in the dual trajectory were configured to match their scans along 3 horizontal virtual lines at 50, 100 and 150 m amsl from 5 km offshore to 4 km onshore. They acquired 45 LOS per virtual line in 45 s, corresponding to a distance between two consecutive points of ≈200 m. Like the sector-scan scenario, the total scanning time amounted to 145 s, including 10 s that the scanner heads need to get back to their starting positions. Radial wind speeds were retrieved separately for each point and lidar and, from these, the horizontal wind speed components were reconstructed over a given period (see below).

To ensure the spatial proximity of two opposite range gates for the dual setup reconstruction, 81 range gates were acquired per line of sight and per system, resulting in the collocated black points depicted in Fig. 3. Detailed information about the pointing accuracy and the measuring volume of the WindScanners is given in Vasiljević (2014).

In order to include all acceptable range-gate combinations, a collocating algorithm filtered out data that did not fulfill a certain range threshold. During phase two, the range gate positions were not well collocated in the x-coordinate (i.e. West-East), and therefore the threshold in the x-direction was set to 51 m. For the y (North-South) and z (height) dimension and in phase three, the threshold was 10 m. The reconstruction algorithm was applied to the 10, 30 and 60-min averaged radial wind speeds of both systems, after filtering out data that did not fulfil a CNR threshold (-26.5 dB). The exact positions of all range gates and phases are given in the RUNE database (Appendix A). The reconstructed 10-min mean values were also added to a high-level database.

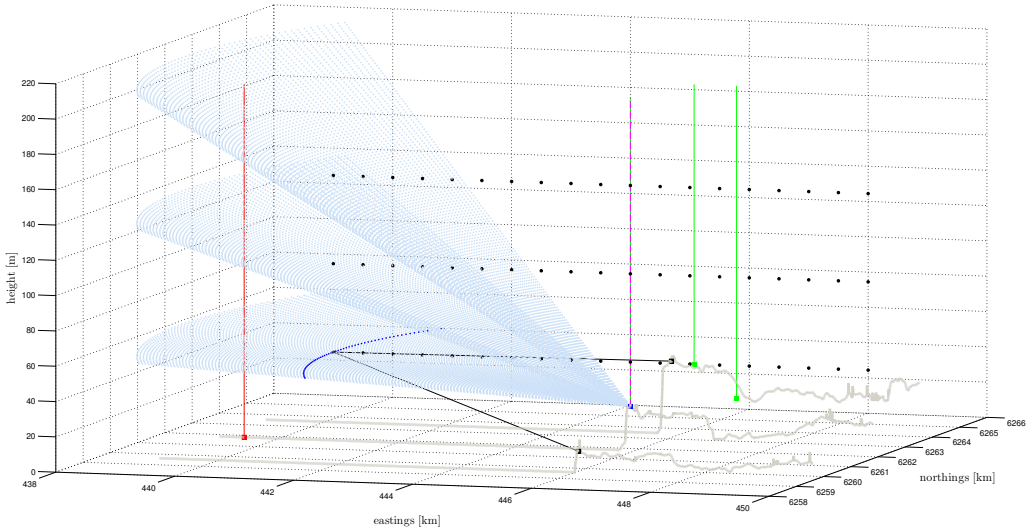

Figure 3. Overview of some sampling points of the RUNE instruments. Collocated points from the dual setup are given in black and the two black lines denote a sample of the two laser beams focusing in the first point of the scanning pattern. The points from the sector-scan are denoted with light blue points, with the dark blue points denoting the first 60° scan that is collocated with the first dual setup point. The green and purple lines denote the position of vertically profiling lidars and the red line denotes the floating lidar buoy in it's first position.

4.2.3 Virtual mast setup

During phase four, Sterenn and Koshava were configured to make dual Range Height Indicator (RHI) scans, i.e. they hold the azimuth angle varying the elevation angle. The azimuth angles of both systems were programmed so that scans were intersecting at 5 km offshore ($x = 440915$ m and $y = 6261837$ m, UTM WGS84, Zone 32V). A vertical profile with ranges at 36 different heights can be obtained (Table 3). For each 10-min interval each height could be sampled 16 times with 1 sec accumulation time. The same reconstruction algorithm and CNR limit was applied as with the dual setup and the 10-min means were finally stored in the high-level database.

4.2.4 Vertical profiling lidars

All heights from the vertically profiling lidars in this section are relative to the height of the lidar. Alizé was configured to measure the whole vertical profile as high as possible. Since the first range gate could not be below 100 m, it was chosen to let the ranges gates vary between 100 and 1500 m. The collocated lidar WLS66 had a first minimum height for the first range gate of 40 m, and so it was configured such that some of the range gates would coincide with the heights of the scanning pattern of the dual setup. With a terrain height of 26 m, the range gates at 74 and 124 m correspond to a height of 100 and 150 m amsl. The same logic was applied for the range gates at a height of 57 and 107 m for 3E and 75 and 125 m for Bura. All range gates from the vertically profiling lidars are given in Table 3.

The sampling time per LOS was ≈3.5, 1, 1, 5, 1 s for Bura, 3E, WLS66, Alizé and the lidar buoy, respectively. All lidars were sampling in 4 positions around the zenith, 90° angularly separated from each other. The zenithal angle of the lidars was ≈30° for the short-range lidars (opening angle of ≈60°) and ≈15° (opening angle of ≈30°) for the long-range lidar. The data were stored in the database as 10-min means and more meta-data can be found in the respective tables of each system (Appendix A).

It was found that the direction offset of Bura during installation was wrong and therefore the data in the database have a 14° clockwise offset. This offset was calculated by performing linear regression between Bura and 3E with a forced slope of 1. The CNR threshold for all profiling

lidars was set to -22 dB, expect for Alizé which had a threshold of -27 dB. This is because of the more powerful laser of the long-range lidar. Only 10-min intervals where all heights up to 130 m above lidar level fulfilled this criterion were used in the analysis.

Name	Max. Range (m)	Range gate height above lidar level (m)
Alizé	1500	100,150,175,200,250,300,350,400,450, every 100 m from 500–1500
Bura	300	30,35,40,50,62,75,87,100,112,125,140,155,175,200,250,300
3E	300	40,57,70,88,107,125,150,200,250,300
WLS66	300	40,50,60,74,80,90,100,110,124,150
Lidar Buoy	300	40,47,59,79,97,117,134,147,172,197,209,247
Name		Range gate height amsl (m)
Virtual mast		5,28,52,75,99,122,146,169,192,217,275,298,322,345,368,392, 415,438,461,486,520,544,568,591,615,639,662,687,710,734, 757,793,816,840,864,888

Table 3. The height of the range gates from the vertically profiling lidar systems and the virtual mast scenario.

The lidar buoy was installed on the 4th of November. On the 15th of November, after a storm, it was found that the blades of the wind-power buoy generators were damaged and the buoy's motion sensor was not working properly. During another storm, the blades were again damaged and the lidar did not have electricity after the 7th of December. Due to the harsh weather conditions it was only possible to relocate the buoy to a better location with less breaking waves by the 11th of February. There, the lidar was measuring more successful until the 30th of March. Detailed documentation about the lidar buoy can be found in Gottschall et al. (2014) and Gottschall (2016).

4.2.5 Wave buoy

A directional wave buoy (Triaxys) equipped with a downward-looking Acoustic Doppler Current Profiler (ADCP) was deployed to measure waves and currents from 4 November 2015 09:00 UTC to 11 January 2016 13:00 UTC at 56° 30.00' N, 007° 59.80' E, where the water depth was 16.5 m. The buoy drifted on 11 January 2016 due to a failing flexible mooring, probably as a result of passing fishing gear. The buoy was recovered on 13 January. The wave buoy data are described in a separate report (Sanchez and Rørbæk, 2016).

4.2.6 Satellite data

Satellite winds from Synthetic Aperture Radars (SAR) and Scatterometers, were collected during the measurement campaign.

Synthetic Aperture Radar (SAR) Synthetic Aperture Radar (SAR) retrievals of 10-m winds were collected from satellites Sentinel-1A and TerraSAR-X during the RUNE experiment. Both sensors are able to measure high resolution wind fields offshore covering large areas.

Sentinel-1A This is a satellite from the European Space Agency (ESA) with an C-band SAR instrument on board circling the Earth on a sun-synchronous polar orbit. It succeeded the Envisat mission and is operational since the end of 2014. During the campaign 41 images were taken from November 2015 to February 2016. Tab. 4 shows when images were acquired.

	1	2	3	4	5	6	7	8	9	10	11	12	13	14	15	16	17	18	19	20	21	22	23	24	25	26	27	28	29	30	31
November	E		M				E						ME					ME		M					ME		M				
December		ME					ME		M			E			M				ME		ME					M					ME
January		E					M					ME		M					M					ME		M			E		M
February					M		E					M					E					M						ME		

Table 4. Dates of the 41 available Sentinel-1A images, M for morning around 6:00 UTC and E for evening around 17:00 UTC

The images are processed using the Geophysical Model Function (GMF) CMOD5.n for VV polarised images and for HH polarised images a correction is applied (Mouche et al., 2005). The wind retrieval yields equivalent neutral wind speeds at 10 m amsl. The SAR scenes are reprocessed with wind direction inputs from the lidars, which give a uniform wind direction for each scene. These directions are regarded to be representative for the relatively small study area (see Fig. 4).

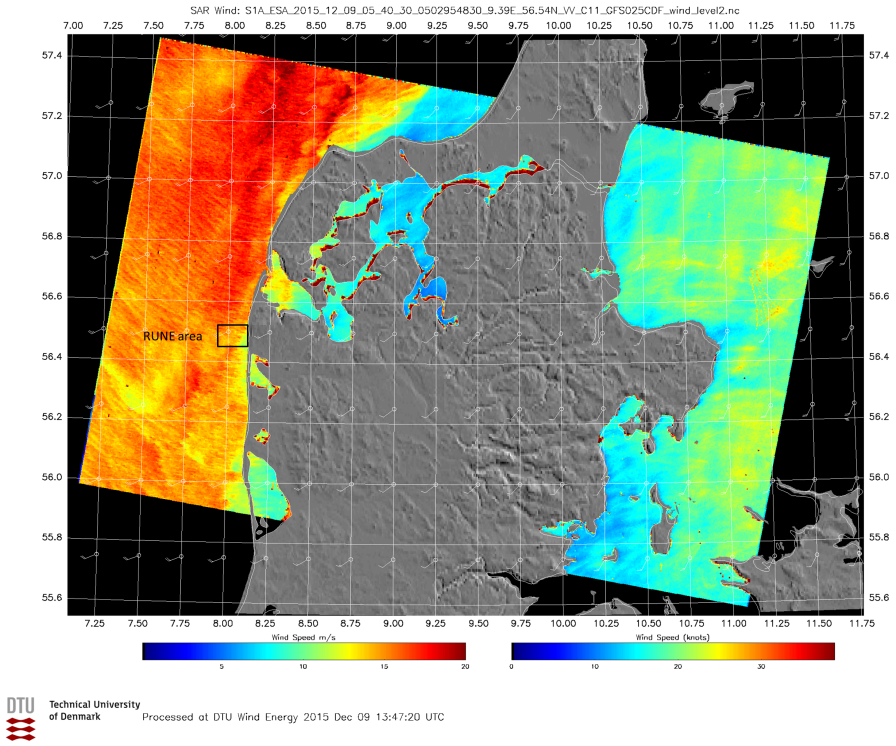

Figure 4. Example of a Sentinel-1A wind map at 5:40 am UTC on 09.12.2016. Wind retrieval for the entire SAR image using GFS model wind speed.

Figure 4 shows a wind field from Sentinel-1A. A front with a clear directional change just moved over the RUNE area. A GFS model wind direction is indicated by the barbs predicting WSW winds. Clearly visible wind streaks west of the RUNE area indicate a wind direction of WNW. Erroneous wind directions from modelled wind directions can cause large deviations in the wind retrieval process. Therefore, a constant wind direction measured from WLS66 was used for the SAR wind retrieval process.

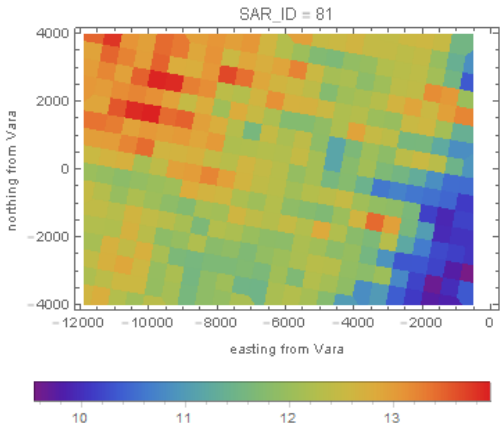

Figure 5. Example of a Sentinel-1A image at 5:40 am UTC on 09.12.2016 zoomed into the RUNE area. Coordinates are compared to the location of Vara. The retrieval is done with a constant wind direction from an onshore profiling lidar.

Fig. 5 shows the wind retrieval from the same day as Fig. 4 zoomed into the RUNE area. The image seems coarse for this small area but it is still possible to obtain information on the coastal gradient of the wind speed.

TerraSAR-X TerraSAR-X (TSX) is an X-band (9.6 GHz) radar operational since 2008, collecting data in three different modes of varying spatial resolution. Radar images have been ordered through a proposal submission procedure, during which the scientific benefits of the RUNE campaign had to be stated. Delivered images are available in two different modes:

- ScanSAR (up to 16 m resolution, scene size of 100 km in width and 150 km in length)
- SpotLight (up to 1 m resolution, scene size of 10 km in width and 5 km in length).

The wind retrieval for TerraSAR-X data is locally performed at DTU Wind Energy, similar to the one for Sentinel-1 SAR images, using the same software (SAROPS) with a different GMF appropriate for X-band radar data. An example of the original brightness image (left) and the retrieved wind (right) is shown in Figure 6.

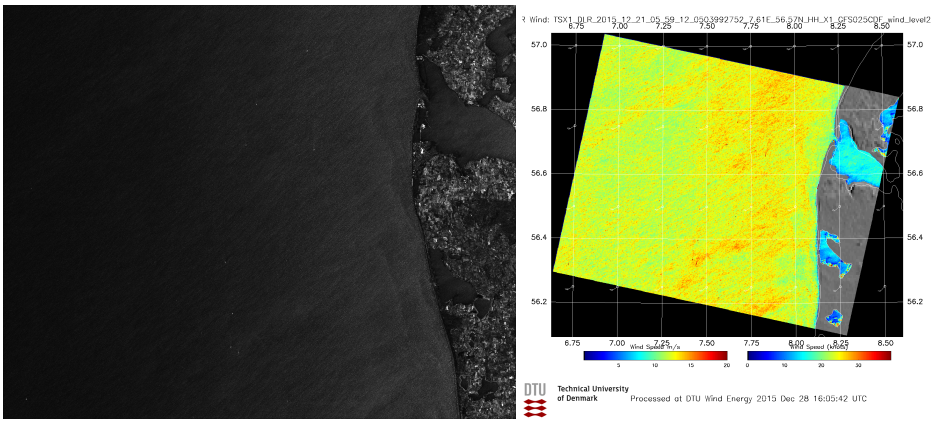

Figure 6. Original brightness radar image (left) and retrieved wind speed (right) on December 21 2015 at 06:00 UTC.

The RUNE campaign offered a unique opportunity to collect and process TSX images for the first time in DTU Wind Energy and therefore, some sensitivity tests regarding the retrieval procedure were performed, especially for the polarization ratio method. As most SAR GMFs are tuned

to vertical polarisation (VV pol) images, the polarisation ratio is applied in the case of horizontal polarisation (HH pol) images. In the case of TSX all acquired images were in HH polarisation and sensitivity tests were performed using two different methods for the polarisation ratio. In addition, due to the very high resolution of the SAR images, averaging of the radar backscatter is required to remove surface signals, such as long waves, that can "contaminate" the wind retrieval process. Three different resolutions were selected for these sensitivity tests and all relevant findings are presented in Section 5.7. TSX data are stored locally on a server and they are easily visible and downloadable through `http://datastation.windenergy.dtu.dk/SatelliteWinds/BrowseData.aspx`. Due to the ordering procedure required for the instrument to collect radar images, not all days during the RUNE campaign are covered by TSX images (see Table 5).

	1	2	3	4	5	6	7	8	9	10	11	12	13	14	15	
November																
December			SP		SP					SC				SC		
January	SC	SP			SC		SC	SP			SC	SC	SP			
February	SP		SC	SP			SC		SC	SP		SP	SC	SC	SP	
	16	17	18	19	20	21	22	23	24	25	26	27	28	29	30	31
November			SP									SP	SP	SP	SP	
December	SC	SP		SP	SC	SC	SP	SC			SC				SP	SC
January	SC		SC			SP		SC	SP			SC		SC	SP	
February			SC		SC	SP		SP		SC	SP			SC		

Table 5. Collected TSX images during the RUNE campaign. SC stands for the ScanSAR mode while SP for the SpotLight mode. Acquisition times are approximately around 06:00 and 17:00 UTC.

ASCAT Scatterometer The Advanced Scatterometer (ASCAT) operates at the C-band (5.255 GHz). From an altitude of 840 km and with 3 antennas it observes the ocean with two 500 km wide swaths, one on each side of the flight path. Wind speed and direction information from ASCAT are freely available and were collected as Level2 (L2) swath winds and Level3 (L3) gridded winds, from the Copernicus Marine Environment Monitoring Service (CMEMS) for the entire period of the RUNE campaign. All data are stored in a local drive. The 12.5 km coastal product was used in both cases, which is specifically developed in order to increase the proximity of wind retrievals to the land.

4.3 Operational availability

The satellite data are available at times given in the previous section. For the ground-based remote sensing instruments, it can be observed from Table 2 that the lidars in Doppler-Beam-Swinging (DBS) mode, profiling lidars, offered a good operational availability compared to scanning lidars, generally above 95%. Vara had a operational availability of ≈80% in a PPI scenario. The synchronised dual scenario had a low availability during phase two due to the damaged scanner-head control unit of Koshava, but had a operational availability of ≈80 % for phase three.

The lidar buoy was damaged by waves, resulting in two months without measurements. When the buoy was recovered, it was moved to a new location but the measurements obtained in March were not concurrent with all other devices.

5 Results

5.1 Wind climate and actual availability

The availability of measurements is determined by the ability of the lidar to measure an accurate radial wind speed, which is mostly a function of the laser power and the presence of aerosols. We define 'actual availability' when all samples within a 10-min interval fulfilled the thresholds discussed in Sect. 4.2. In the top panel of Fig. 7, the actual availability of the measurements systems is shown.

It should be noted that the measurements of the scanning lidars during phase one have not been written to a high-level database yet. Also the sector scan during phase four is not available as high-level database and therefore not shown. However, data from these periods can still be accessed (Appendix A).

For the sector scan during phase 2 and 3 and for the dual setup during phase 2–4 all data where a range at any distance fulfilled the CNR criteria have been marked as available, but data where all range gates fulfil that criteria are rarer. The lidar buoy was not available for a long period and measured until the end of March when all instruments had stopped measuring.

The RUNE campaign was generally characterized by very windy weather with sustained winds from the west. The middle panel shows the wind speeds at the Høvsøre metmast at 100 m. It can be seen that there are several occasions where wind speeds reach more than 24 $\mathrm{m\,s^{-1}}$, which are classified as 'storms' in Denmark. Particularly during November and December it was very windy, with a maximum wind speed of 35.3 $\mathrm{m\,s^{-1}}$ at 18:30:00 UTC on the 29th of November.

The wind direction (lowest panel) shows that the wind speed was mainly from westerly directions during November and December and then a period of several weeks with mostly easterlies followed. It seems that during this period with 'clean' arctic air from the east the atmosphere had relatively few aerosols and, therefore, 3E, Bura and the scanning lidars had no data that fulfilled the CNR threshold up to 130 m.

In Fig. 8 the operational availability is taken as 100% and the actual availability as a function of distance is shown. It can be seen that availability drops when the sampling points are further away from the devices. This is true when moving along the x-coordinate and it can also be seen that the sampling points from the highest level 3 generally have the lowest availability. Furthermore, availability from the dual setup is slightly lower than the sector-scan setup, because Koshava and Sterenn covered additional distance because their position is not collocated with Vara (Fig. 2). The points over land with very low availability are due to the laser beam hitting an object.

In Fig. 9 we match all vertically profiling lidars fulfilling the CNR thresholds with the data from a cup anemometer on the Høvsøre meteorological mast at 100 m. This results in 5665 available 10-min intervals. The mean wind speed $\overline{U}$ from Bura is 13.6 $\mathrm{m\,s^{-1}}$ and is slightly higher than that obtained from Høvsøre ($\overline{U} = 13.5$ $\mathrm{m\,s^{-1}}$). This could be due to the terrain height which is slightly higher or due to the fact that Bura is closer to the coast. Generally we expect increasing mean wind speeds when moving westwards. A linear regression fitted through the origin shows a Pearson correlation coefficient $R^2 = 0.93$.

In Fig. 9 (top right) the wind speed from the slightly more westerly located lidar 3E versus those obtained from the Høvsøre metmast at 100 m are shown. The mean wind speed here is significantly higher, because 3E is located at a 43 m amsl. It does not have a range gate at 100 m either, which is why we used the range gate at 88 m above ground level (agl). At that height, $\overline{U} = 14.0$ $\mathrm{m\,s^{-1}}$ and $R^2 = 0.96$. In Fig. 9 (bottom left and right) we show the wind speed of WLS66 and Alizé, which are in the same location. WLS66 shows that $\overline{U} = 14.3$ $\mathrm{m\,s^{-1}}$ and $R^2 = 0.96$, whereas for Alize $\overline{U} = 14.5$ $\mathrm{m\,s^{-1}}$ and $R^2 = 0.97$.

5.2 Comparison of wind speeds between vertical profilers

To have an impression of the quality of the data of two lidars that measure next to each other, Fig. 10 (left) shows the 10-min mean wind speeds obtained from WLS66 and Alizé. It can be

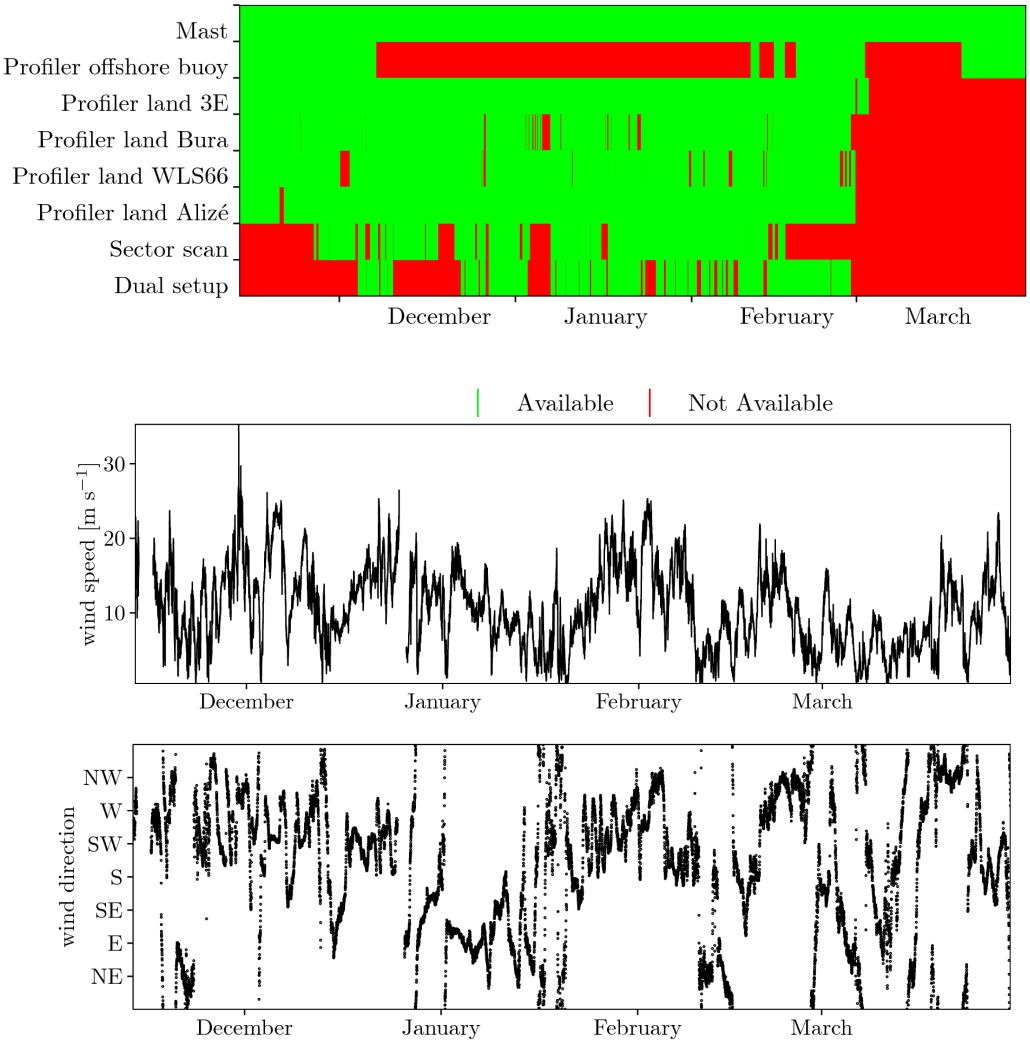

Figure 7. Actual availability of all instruments measuring wind speeds at RUNE after filtering and reconstruction (top panel). The wind speed (middle panel) and the wind direction (bottom panel) at 100 m from the Høvsøre meteorological mast measurements during the campaign are also shown. The dashed line in the middle panel denotes the wind speed which in Denmark is classified as storm (24 m s^{-1}). The Greenwhich Mean Time zone is used for the time axis.

seen that agreement is generally good (Pearson's correlation coefficient $R^2 = 0.99$), but there are some significant outliers. There is generally a small positive bias in wind speed, with a slope of the linear regression line fitted through the origin of 1.03. The reason for this bias is yet unknown, but it could be related to the difference in measuring volumes and flow inhomogeneity near the cliff. The zenithal angles are 28° and 15° for WLS66 and Alizé, respectively, so the horizontal measuring area of WLS66 is significantly larger at 100 m.

Although 3E and Bura are separated about 500 m, the wind speeds from both devices agree well. Using linear regression fitted through the origin, a slope of 1.01 and $R^2 = 0.97$ are found. Despite the CNR filtering, there is also some outliers here, where Bura shows much lower wind speeds than 3E. All these outliers, also shown when comparing Bura to the Høvsøre meteorological mast measurements, were measured during sub-zero temperatures, implying that they might be related to cold weather conditions.

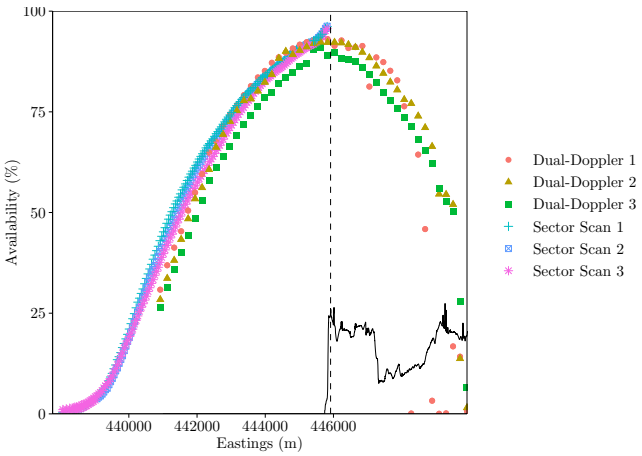

Figure 8. The actual availability as a function of horizontal position along a transect. The numbers refer to the first, second and third level of measurements from the two setups. The dashed line indicates the approximate position of the devices and the solid line is the height of the terrain (not on scale).

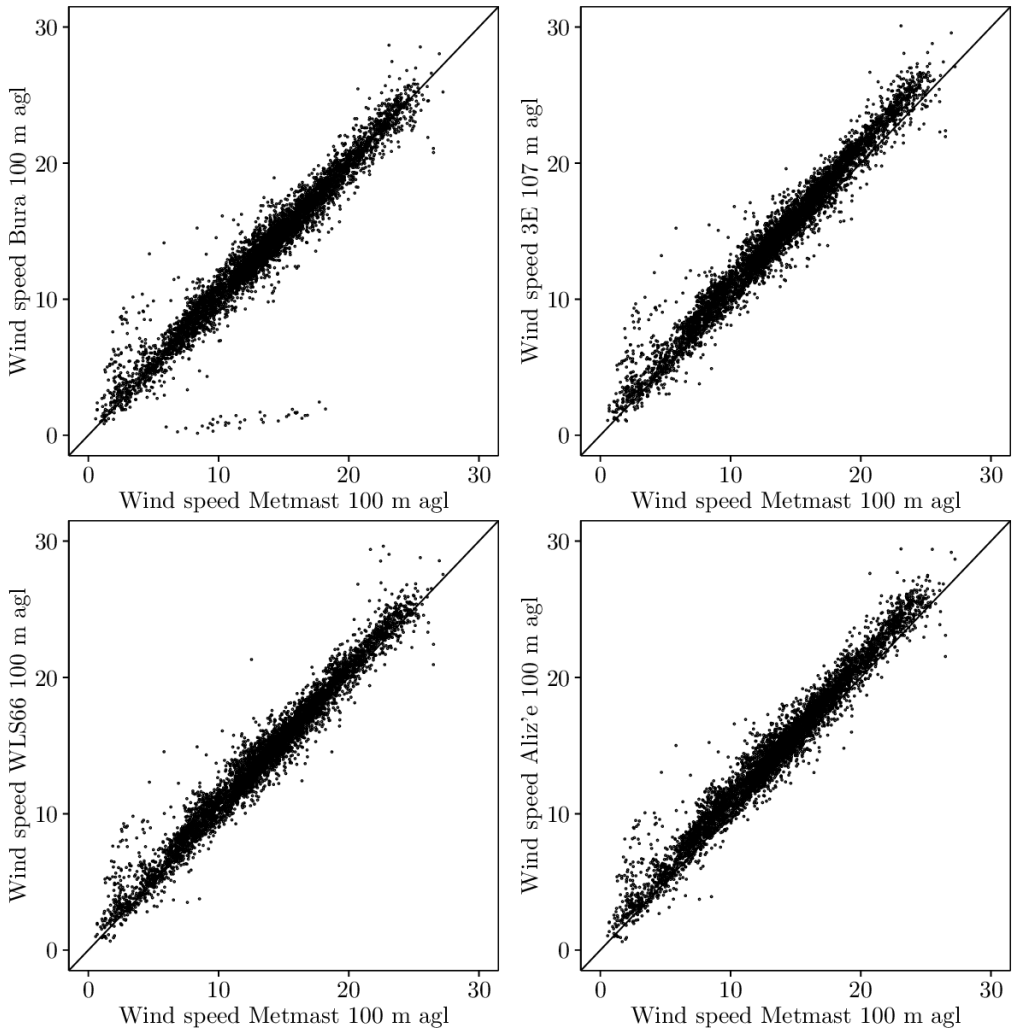

Figure 9. The 10-min mean wind speeds from the vertically profiling lidars compared with those from the Høvsøre meteorological mast at ≈100 m above ground level and a line through the origin with a slope of 1.

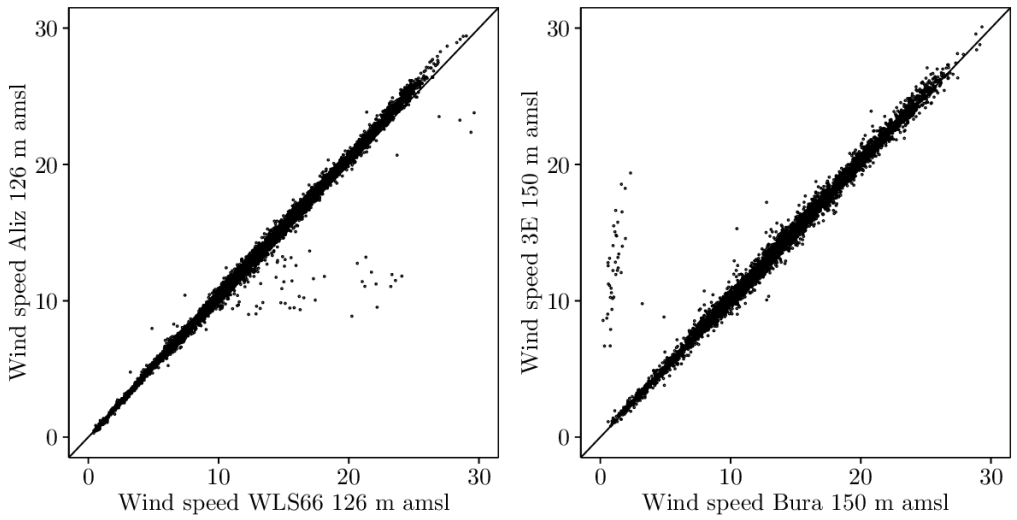

Figure 10. The 10-min mean wind speeds at ≈150 m amsl and a line through the origin with a slope of 1 from the vertically profiling lidars WLS66 and Alizé (left) and from Bura and 3E (right).

5.3 Comparison of wind speeds between the dual setup and vertical profilers

Here we use all data where there was 100 % availability for the dual setup in the chosen range gate and merge those data with the filtered data from Bura. Unfortunately there is no longitudinal point where the profilers can be exactly compared with a point on the transect from the dual setup: the closest point next to WLS66 and Alizé is 100 m to the west of their position, just at the position of the cliff, and there is one 100 m further to the east of their position. In addition, the terrain in this area is quite complex.

Therefore, we compare a scan inland from the dual setup with Bura, despite Bura being located more to the North at a slightly different terrain elevation (Table 1). It can be seen in Fig. 11 that the same outliers are visible as in Fig. 9 (top left) and 10 (right), caused by the measuring errors of Bura. This comparison shows slightly more scatter and linear regression fitted through the origin gives a slope of 1.06 and $R^2 = 0.95$. This is partly due to the effect that there is only 4 samples of the dual setup for a 10 minute interval, whereas Bura measures every 4 s in the same 10-min interval. $\overline{U} = 12.0\ \mathrm{m\,s^{-1}}$ for Bura and $\overline{U} = 12.8\ \mathrm{m\,s^{-1}}$ for the dual setup.

5.4 Comparison of wind speeds between the sector-scan and dual setup

There is only a limited amount of positions where the scanning pattern from the dual and the sector-scan setup intersect. Even at these intersecting positions, we do not expect the 10-min wind speeds to be exactly the same. This is because of the different size of the measuring volume and due to the inherent spatial and temporal variability of the wind speed. The scanning pattern was chosen such that at ≈5 km offshore, the sector-scan and the dual setup measure at nearly the same heights of 50, 100 and 150 m amsl. Furthermore, there are intersecting points at 50 m height, ≈0.9 and 1.7 km offshore and at 100 m, 2.7 km offshore.

In Fig. 12 the 10-min mean wind speeds from the sector-scan and dual setups during phase 3 and 4 are shown. In this section we use only data with 50% or higher availability within a 10-min interval, because using an availability of 100% highly reduces the number of observations at long distance from the scanning lidars. Consequently the number of 10-min observations is 4964, 4605, 1325, 1218, 1204 for panels a–e, respectively. Panels a) and b) show the wind speed at ≈ 900 and 1700 m offshore, respectively. The agreement is good (Pearson $R^2 = 0.97$), but there

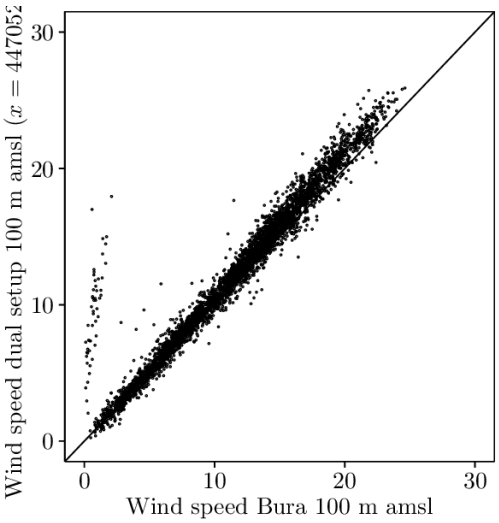

Figure 11. The 10-min mean wind speeds from Bura and the dual setup ($x = 447052$ m) at ≈100 m amsl and a line through the origin with a slope of 1.

appears to be a cluster of points where the sector-scan has higher wind speeds. The slope of the line forced through the origin with linear regression is 1.00 for a) and b).

For the comparison at 5-km offshore at 50, 100 and 150 m amsl (panels c–e), the agreement is also good, but the slope of linear regression through the origin is 1.02, leading to a small positive bias in mean wind speed of ≈0.3 m s^{-1} (≈2 %). The Pearson correlation coefficient is also somewhat lower than closer to the shore (0.86, 0.88 and 0.83 for 50, 100 and 150 m, respectively), because the spatial averaging is proportional to the radius of the circle for a given azimuthal opening angle.

The reconstruction of the wind speed from the sector scan will be most difficult when the wind direction is from the South or North. The radial wind speed will be low, because the sector scan is pointing in a westerly direction. Therefore, in Fig. 13 we have plotted the mean and standard deviation of the difference between the wind speed from the dual and the sector-scan setup at 50 m amsl as a function of wind direction. The wind direction was determined from the vertically profiling lidar WLS66, because it had the highest actual availability.

In Fig. 13 we can determine the sectors, where a bias or higher uncertainty in reconstructed wind speed occurs. For the points closest to coast ($x = 445011$ m and $x = 444193$ m), the bias and standard deviation are indeed highest in the southerly direction, although this only leads to a bias of ≈ 0.3 m s^{-1}. For the point nearly 5 km offshore, there is a bias in mean wind speed for the southerly and southwesterly sector of more than 1 m s^{-1}. It is not clear which mechanism is responsible for the bias in the southwesterly sector.

5.5 Comparison of virtual mast with and the lidar buoy wind speed measurements

Here we compare the RHI scenario of the dual setup with the lidar mounted on the buoy. More data of the lidar buoy are shown in Gottschall et al. (2014). In the latter study it was found that the wind direction has to be corrected for the influence of waves, but that the wind speed does not need a correction. Because of the location of the buoy is ≈5 km offshore, both scanning lidars have to cover large distances, which drastically reduces the amount of available data.

When requiring 100% availability for the RHI scenario, there is only 0-20 available 10-min intervals at most of the heights during phase 4. Therefore here we include only intervals with an availability of at least 50%, i.e. where at least 8 of the 16 samples in a 10-minute interval fulfil the CNR-threshold. The wind speeds at 100 m amsl from the lidar buoy are compared with those from the dual setup (Fig. 14). Linear regression fitted through the origin shows that $R^2 = 0.96$

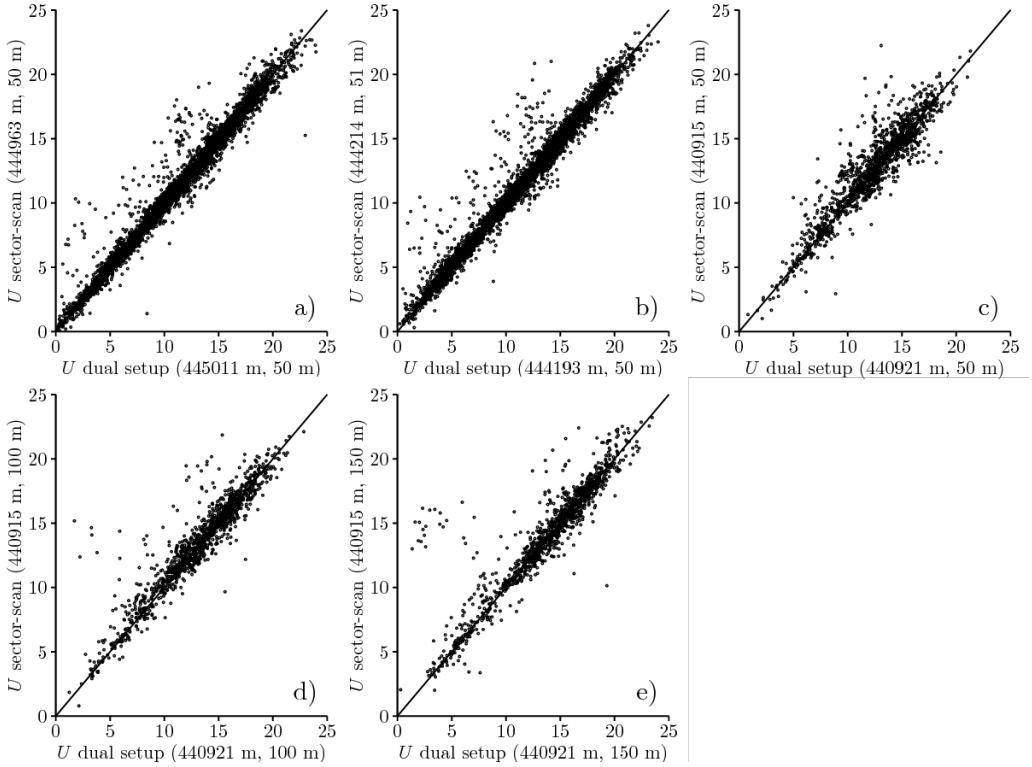

Figure 12. The 10-min mean wind speeds from the sector-scan and dual setup (black points) and a line through the origin with a slope of 1.

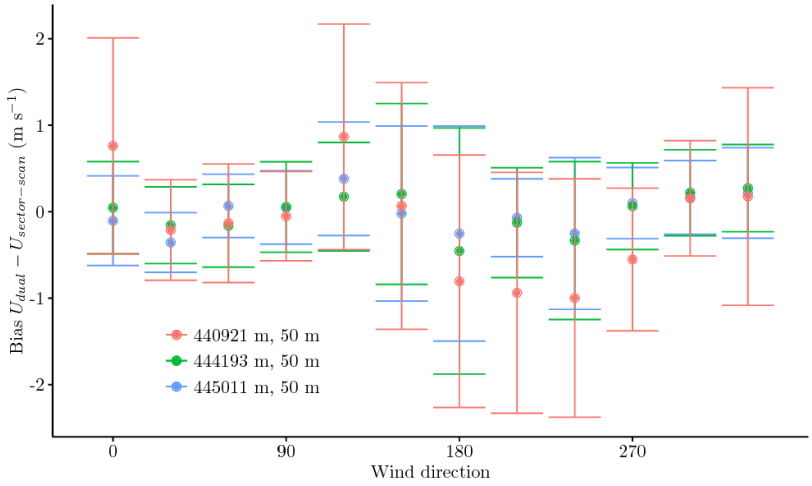

Figure 13. The mean (coloured point) and standard deviation (coloured error bars) of the difference between 10-min mean wind speeds from the dual and the sector-scan setup at 50 m amsl and three different horizontal position in west-east direction.

with a slope of 1. For the dual setup $\overline{U} = 12.5$ m s^{-1} and for the lidar buoy $\overline{U} = 12.6$ m s^{-1}. Lowering the availability criterion of the virtual mast to values lower than 50% increases the amount of available measurements, but also introduces wind speeds that are clearly wrong (e.g. $U > 60$ m s^{-1}).

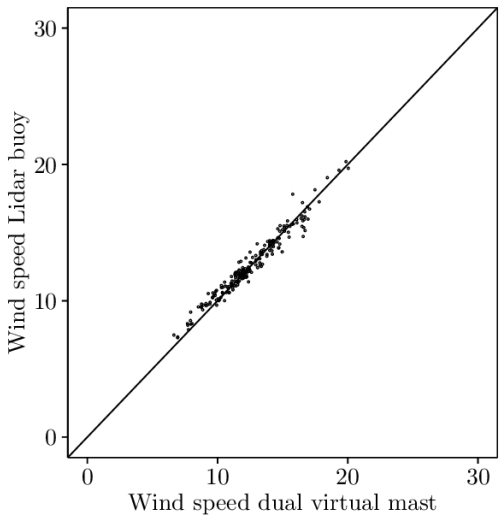

Figure 14. The 10-min mean wind speeds at 100 m amsl from the virtual mast scenario of the dual setup and the wind speed from the lidar buoy (black points) and a line through the origin with a slope of 1.

5.6 Mean wind speed transect of all instruments

To be able to compare transects of mean wind speed across the coast, we need concurrent measurements that fulfill the CNR threshold at all positions. Otherwise the mean wind speed would depend on the availability, because we sample from a different distribution at each point. Since the points from the sector-scan are not sampled at a constant height, we focus here on the dual setup. We use the mean wind speed from the sector-scan and from the vertical profilers when available at the same height as the dual setup. The lidar buoy is not used, as it is usually not concurrently available with all other measurements.

Fig. 15 (top panel) shows the mean wind speed from all sampling points from a distance of 5000 m offshore to 1500 m inland that had at least one sampling point available that fulfilled the CNR threshold in each 10-min interval for the dual and sector-scan setups. This results in 831 combined 10-min transects that fulfill the chosen filtering limits when combining the datasets from all devices, including the vertical profilers on land. Requiring 100% availability would reduce the number of transects to only 37. In Fig. 15 (bottom panel) we reduce the distance up to which we require our filtering and use 2429 10-min intervals between 2000 m offshore and 1500 m inland.

It can be seen that the mean wind speed gradually decreases moving towards the coast, mostly so at 50 m. At the coastline, we observe a large increase in mean wind speed, mostly at 100 and 150 m. The mean wind speed observed with the vertically profiling lidars is slightly lower than that from the dual setup. For 3E this might be because the distance to the ground is lower but it should be note that the transect is not at the same latitude where Bura and 3E are installed.

At 700 and 1900 m offshore, the mean wind speed from the sector-scan agree well with that from the dual setup. At 5 km, the mean wind speed of the sector-scan is higher than that from the dual setup, as discussed in Sect. 5.4.

5.7 Comparison between scanning lidar measurements and satellite data

The three long range Windscanners are suitable for comparisons of SAR and lidar, (see Sects. 4.2.1 and 4.2.2). Lidar and SAR use fundamentally different physical phenomena to measure the wind speed. Attempts of comparing these datasets should take this into account. The GMF infers SAR wind speeds at 10 m with spatial averages depending on the resolution of the processing.

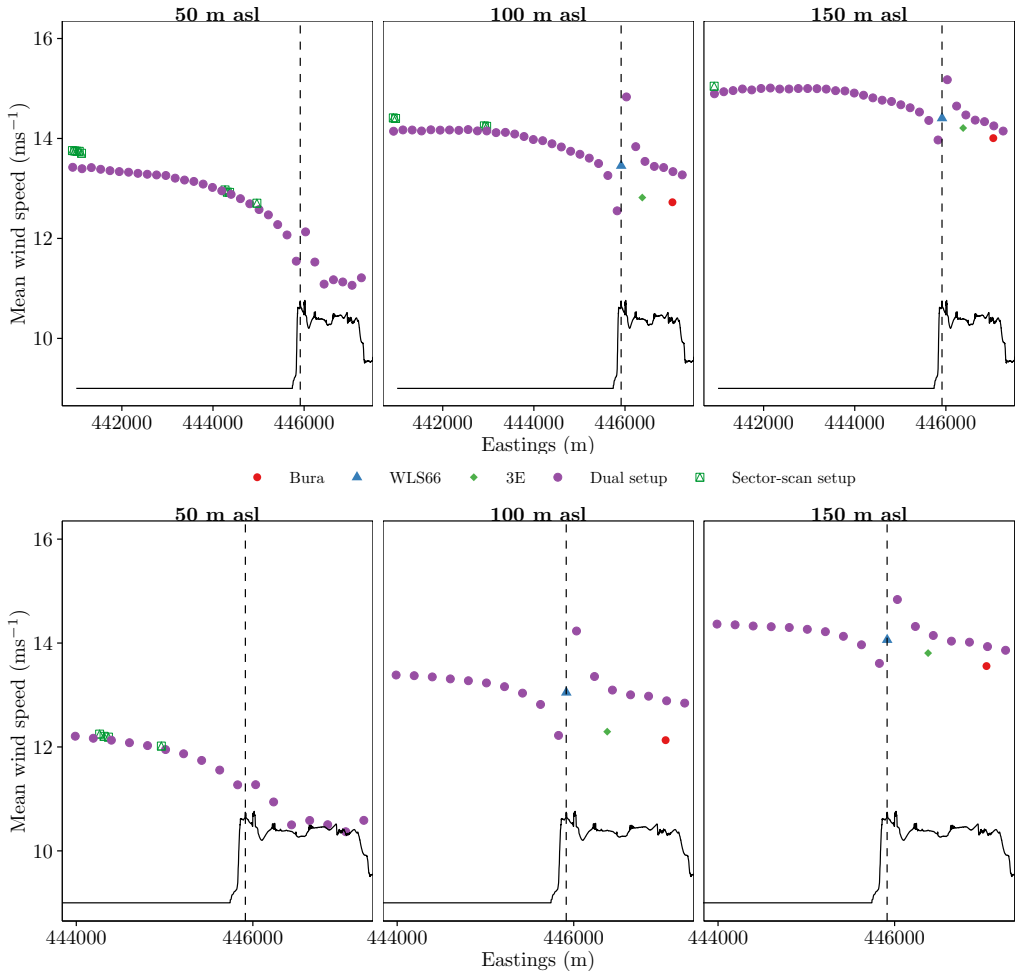

Figure 15. The mean wind speed of all full transects of 10-min observations from the dual setup (purple points), concurrent measurements from the sector-scan setup (green points) and from the vertically profiling lidars at 50, 100 and 150 m amsl. The black solid line denotes the terrain height (not on scale). The upper panel includes full transects from 5000 m offshore to 1500 m inland, whereas for the lower panel the distance is 2000 m offshore to 1500 m inland.

The dual setup can give almost instantaneous wind speed reconstructions for a small measuring volume, whereas the sector scan setup has some spatial averaging applied in the reconstruction of wind speeds. To make lidar and SAR comparable, the wind speed from the lidars is extrapolated down to 10-m amsl. A version of the Charnock wind profile (Fairall et al., 2003) is used for the extrapolation. Their wind profile is applicable to mean wind speeds and therefore, 10-min averages of the reconstructed lidar wind speeds are used.

5.7.1 Sentinel-1

For Sentinel-1, CMOD5-n infers wind speeds at 10 m using spatial averages of 500 m $\times$ 500 m. Additionally, the SAR wind speed is spatially averaged 2 km north and south of the transsects assuming homogeneity along the coast. 28 Sentinel images have been taken during phase 2 and 3. Dual Doppler 10 minute averages are available for 10 cases (see Section 4.2.2) and sector scan reconstructions are available for 12 cases (see Section 4.2.2). A logarithmic wind profile using the Charnock relation is used to extrapolate the lowest level of the lidar measurements down to 10 m. Comparisons of the individual cases show some good agreement but also differences of more than 3 m s^{-1}.

Fig. 16 shows that the difference of 10-m wind speeds from the dual setup and SAR is less

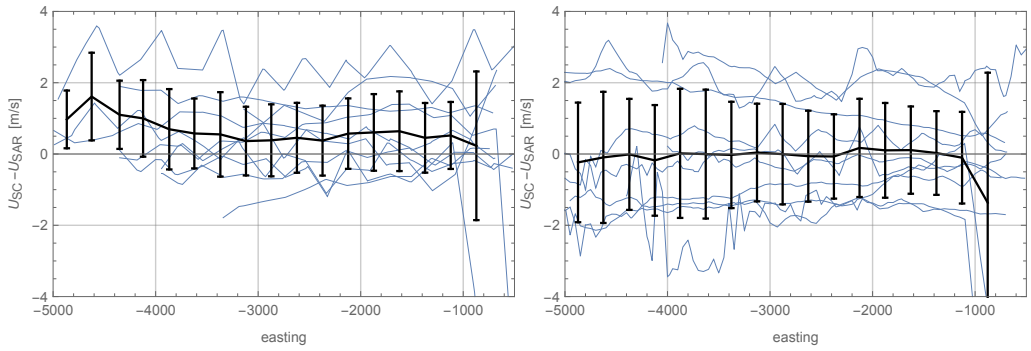

Figure 16. Comparisons of the estimated 10 m wind speed from SAR and 10 m extrapolated winds from: Left – reconstructed dual Doppler at 50 m, right – reconstructed sector scans on the lowest level. Blue: individual cases, black: mean over all cases with stadar deviation in each bin.

than 2 m s^{-1} for most cases. The average bias over the transect is 0.7 m s^{-1} with an RMSE of 1 m s^{-1}. The comparison between SAR and sector-scans have some cases with deviations of more than 2 m s^{-1}. The mean bias over the transect is almost zero and the RMSE is 1.46 m s^{-1}.

Differences in the temporal and spatial averaging between lidars and SAR are likely to account for deviations in the wind speeds. Additionally, the extrapolation of wind speed adds uncertainty because influences from e.g. stability, internal boundary layers or low level jets are not taken into account. A more accurate assessment of the quality of SAR winds will need a more thorough investigation of each case.

5.7.2 TerraSAR-X

For the TerraSAR-X comparisons with the dual doppler lidar scans, the same procedure for extrapolation down to 10 m as for Sentinel-1 is used. For the comparisons, the 10-min dual Doppler transect closest to the TSX overpass time is selected; the TSX wind speed at the minimum distance from the lidar points are selected from the entire wind field. As mentioned in Section 4.2.6, wind retrievals from the TSX radar images were derived for the first time at DTU Wind Energy during the RUNE campaign. Due to the very high spatial resolution and the acquired image polarization, sensitivity tests were performed with two different varying parameters. The polarization ratio methods of Thompson et al. (1998) and Li and Lehner (2014) were used, while the original radar images were averaged in grid cells of 60, 200 and 500 m prior to the wind retrieval.

The sensitivity of the retrieved wind to the different parameters used for the retrieval procedure, was evaluated for the different combinations and polarisation ratios. It is presented in the form of density scatterplots, in Fig. 17, for the 3 different resolutions. The mean bias (μ) between the two polarisation ratios, is small and less than 0.1 m s^{-1} for all resolutions. The standard deviation (σ) is around 0.5 m s^{-1} and relatively constant for the 3 resolutions, which is also the case for the correlation coefficient r, being higher than 0.9 for all different resolutions. While there is a good agreement of the 2 polarisation ratios for all spatial resolutions and for wind speeds ranging between 5 and 14 m s^{-1} (where most data exist), there seems to be a tendency for the Thompson et al. (1998) polarisation ratio to overestimate the wind speed for winds higher than 30 m s^{-1}.

An example of the comparison between the TSX retrieved transect for varying resolutions (different colours) and polarisation ratios (diamonds vs squares) matching the dual setup transect (grey solid line) is shown in Fig. 18, for the wind speed (left) and the wind direction (right), on January 13 2016. The 50 m dual setup wind speeds were extrapolated to 10 m using a constant roughness of 0.0002 m. Overall, and for this case, the difference in wind speed is smaller when the Thompson et al. (1998) polarisation ratio is used (squares). The dual setup shows variability of the wind speed from the coast and up to 4.5 km offshore, which is also seen in the TSX retrieved winds. The lower resolution wind retrievals (500 m, green) provide only 3 points within 5 km from the land, and thus are not very helpful in this case. The wind direction comparison

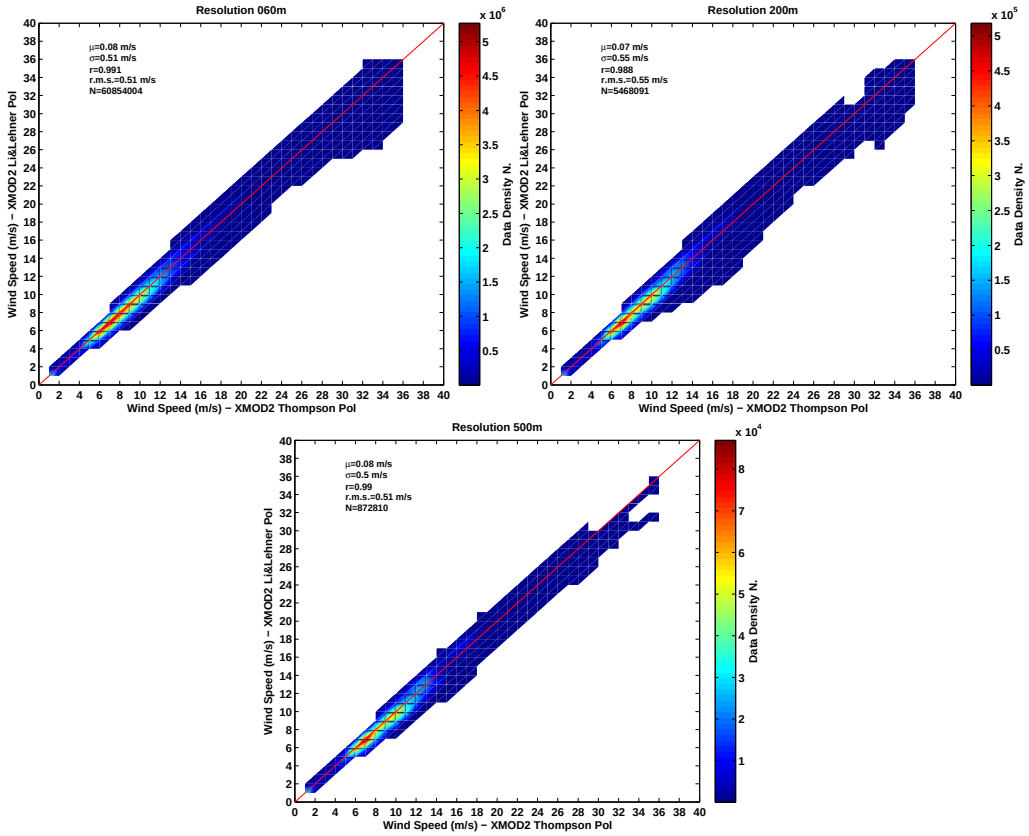

Figure 17. Scatterplot of wind speed between the Thompson et al. (1998) (x-axis) and Li and Lehner (2014) (y-axis) polarisation ratios, for spatial resolutions of 60 m (top), 200 m (middle) and 500 m (bottom).

(right) shows that the GFS model wind direction used for the wind retrieval is almost constant from the coast and up to 4.5 km offshore, at ∼45°, while the dual setup wind direction varies between 36 and 46°.

The overall statistics between the dual setup and TSX retrieved with different combinations of the polarisation ratio and the spatial resolution for the available cases are presented in Fig. 19. The colour lines represent different cases of available match-ups between the dual setup and the TSX transects. The mean bias (top left) is generally large and in the order of 2 m s^{-1}, independent of spatial resolution and polarisation ratio (*x*-axis). For a couple of cases (27/01 and 07/02) the bias and RMS error (top right) are very large. For these particular cases, the wind direction bias and RMS (right panel) are relatively low, compared to other cases, and in the order of 15°. The correlation coefficient for the wind speed (Fig. 19, bottom right) is generally low and for some cases negative, but for the wind direction (not presented) the trend is more obvious. Correlation is higher than 0.5 and for some cases close to 0.9 but there is a tendency for negative correlation as well. The number of match-ups decreases for decreasing resolution, as expected.

The wind directions used for the TSX wind speed retrievals, were obtained from the GFS model, which due to its resolution provides a single value for the area covered by the lidar transects. For the cases investigated, the wind direction from the model was not differing by more than 15°, but the variability was not captured.

In summary, the sensitivity tests performed on the methods for the wind speed retrieval showed small differences in the statistics for the different combinations of the spatial resolution and the polarisation ratio.

Overall, it can be concluded that while the TerraSAR-X data are helpful for the comparisons with the lidar scans due to their high resolution, more tests need to be performed before concluding the final setup for the wind retrieval process. Nonetheless, it should be highlighted that

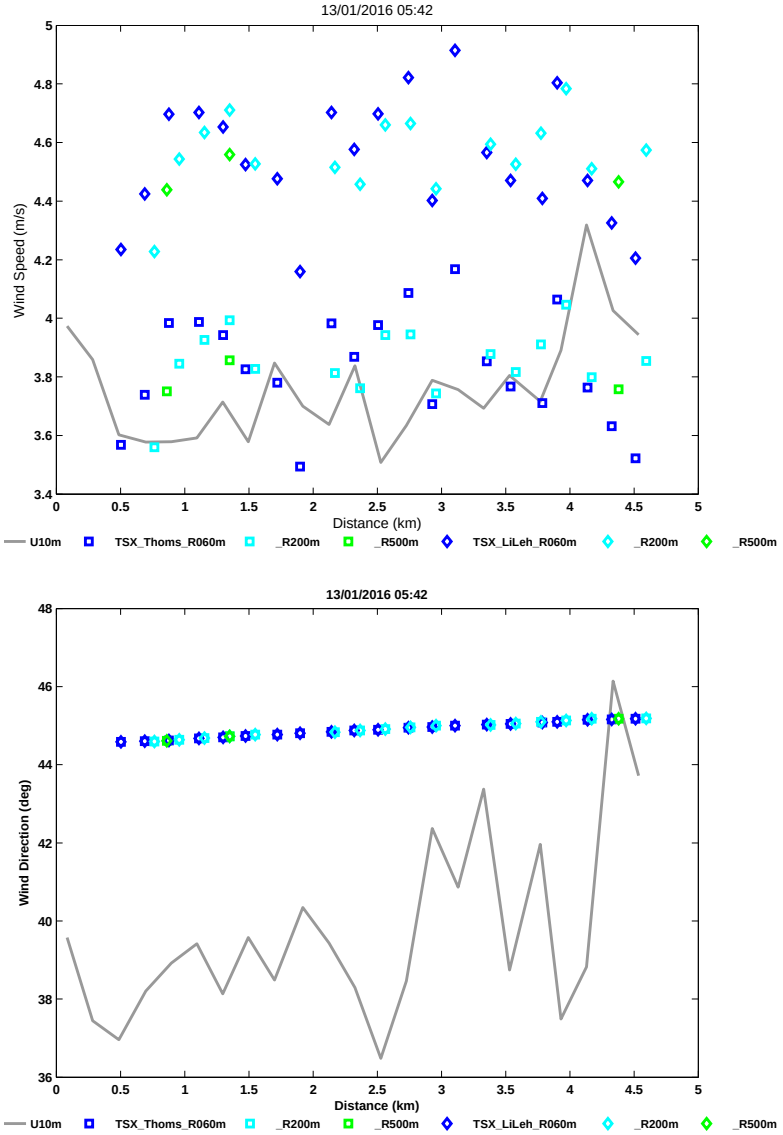

Figure 18. Wind speed (top) and direction (bottom) for a transect of a TSX image (SpotLight Mode) matching the dual setup reconstruction (gray line).

the lidar transects used for the comparisons, are not the original ones, but extrapolated values assuming neutral stability. While for certain cases this may be a good approximation (when the comparisons yield low bias and RMSE), for others such an assumption may not be valid. More insight on such matters are expected with the utilisation of the PPI scans.

5.7.3 ASCAT

The ASCAT L2 winds (see left panel in Fig.20) were consistently retrieved further away from the reach of the dual Doppler and sector scanning lidars, at least for the period evaluated. Nonetheless, these retrievals can be used for validation with models at this part of the ocean where in situ measurements are not available. The L3 gridded winds, an example of which can be seen in the right panel of Fig. 20, cover the area of the RUNE measurement campaign and can be used for comparisons with, potentially, all the lidar scans and model outputs.

No direct comparisons of ASCAT retrievals with the lidar data have been performed up to now, but the data can be used to validate offshore model outputs and compared with the PPI scanning

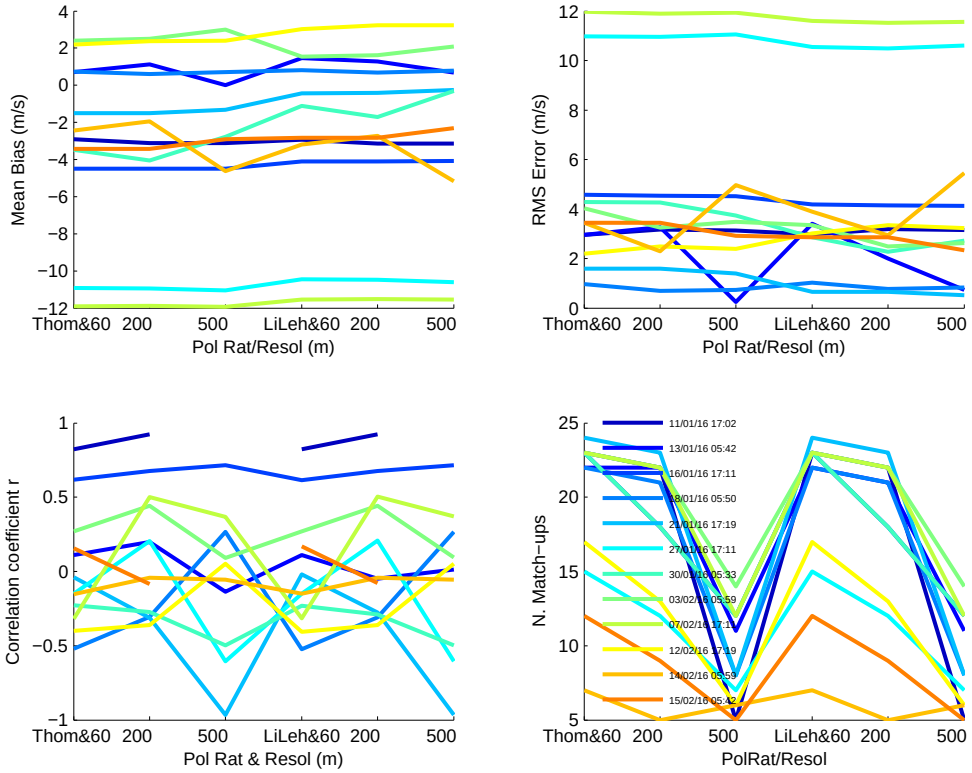

Figure 19. Statistics of the wind speed differences between the dual setup transect and the TerraSar-X retrieved winds as a function of the different spatial resolutions and polarization ratios (x-axis), for the different match-up cases (coloured lines).

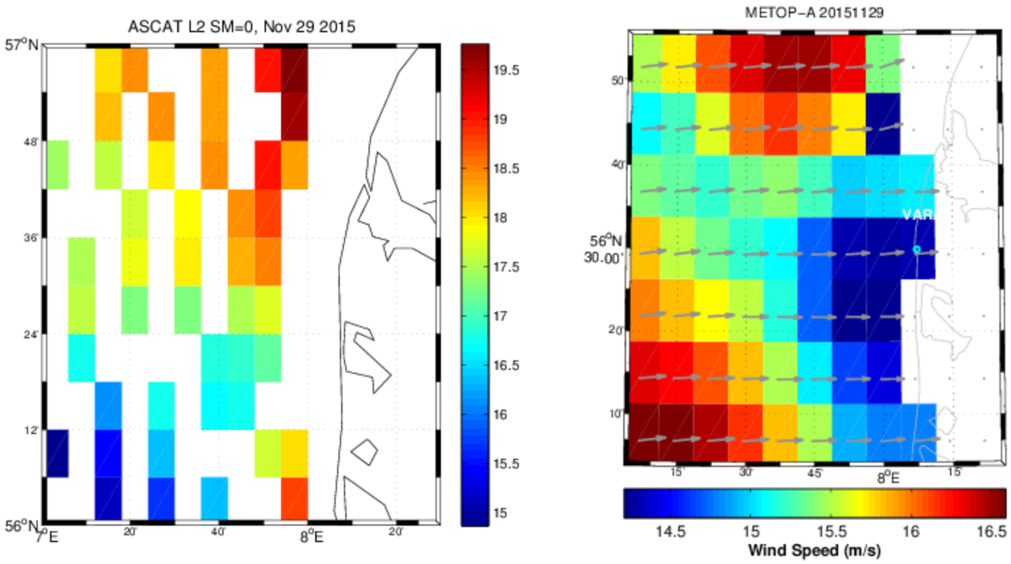

Figure 20. Example of ASCAT L2 swath winds (left) and L3 gridded winds (right) retrieved on November 29, 2015.

scenario and the mean wind speed transects. Figure 21 shows the ASCAT mean wind speed over the entire period of the measurement campaign for a transect starting from the point closest to Vara and up to ∼65 km offshore. The data availability ranges from 240 wind retrievals offshore, down to 189 retrievals 13 km offshore and 63 retrievals, 7.5 km offshore. Nonetheless, a wind speed gradient at 10 m above the surface is captured, with a reduction of almost 1 $\mathrm{m\,s^{-1}}$ towards the shore.

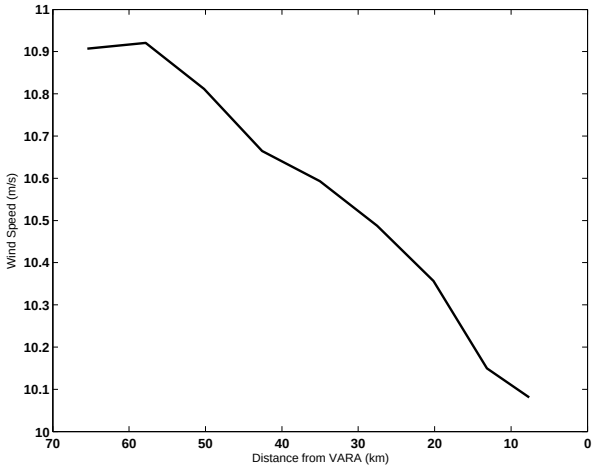

Figure 21. ASCAT L3 gridded mean wind speed transect for the entire period of the measurement campaign. The transect represents the mean wind speed gradient from the point closest to Vara, ∼ 7.5 km offshore, and out to a distance of ∼65 km.

From this, it can be speculated that the 12.5-km resolution of the retrieved winds is probably not going to allow for any direct comparisons with the dual and sector-scan setup, as the entire scanning area offshore coincides with a specific ASCAT grid point. Nonetheless, more investigations need to be performed.

6 Conclusions

The RUNE campaign has resulted in detailed novel measurements of the flow in the coastal zone. The flow during the campaign was mostly westerly, with higher wind speeds than usual in this time of the year and the occurrence of several storms. The availability of 4 land-based vertical profilers was the highest, generally above 95%. The sector-scan and dual setups had a lower availability for longer distances due to the decrease in backscatter signal. The virtual mast scenario had the lowest availability of the scanning setups, because it was located at ≈ 5 km. The energy supply of the lidar buoy was damaged by waves several times and experienced long periods of unavailability as well.

We inter-compared the different measurement systems, taking the Høvsøre meteorological mast as a reference. As expected the wind speed was decreasing when moving from the shoreline inland. Comparison with two vertically profiling systems that were collocated showed that, apart from a short period in January, agreement was excellent. Two profiling lidars that were seperated 500 m horizontally showed slightly more scatter. The dual setup compared well with a vertically profiling lidar, despite the largely different sampling rates and measurement volumes.

The mean wind speed from the sector-scan showed good agreement compared with the dual setup near the coast, but had a positive bias at 5 km offshore. This can be related to uncertainty in the wind speed reconstruction for situations with low radial wind speeds, as the bias was largest for winds from the southerly sector. The reconstructed winds speeds from the virtual mast scenario compared well with those obtained from the lidar buoy. However, the number of samples was very limited due to the long distance from the devices performing the virtual mast scenario to the buoy.

Satellite winds from different sensors were also retrieved during the RUNE campaign. Scatterometer winds from ASCAT were of coarse resolution for any direct comparisons with the lidar measurements. A mean wind speed gradient was present in ASCAT and with further refinements some meaningful comparisons could be achieved.

SAR retrieved winds with high spatial resolution and have been used for direct comparisons with the lidar scans. The lidar data is not measured at 10 m and a logarithmic profile with the Charnock relation has been used. An RMSE between 1 $\mathrm{m\,s^{-1}}$ for the comparison with the dual Doppler setup and 1.5 $\mathrm{m\,s^{-1}}$ for that with the sector scans was found, which is similar to the performance of CMOD5.n compared to offshore met masts Hasager et al. (2015) indicating the usefulness of Sentinel-1 wind retrievals close to the coastal zone.

TerraSAR-X retrieved winds showed a rather large deviation from the extrapolated lidar transects, mostly for the wind speed. The wind speed variability with the distance from land was well resolved in almost all the cases. Overall, the TerraSAR-X wind retrievals can offer a valuable source for direct comparisons with the lidar measurements but further research related to the wind retrieval procedure is required.

A Database structure

The data of all instruments from the RUNE campaign is stored in a database called “RUNE” (IP-address 130.226.56.234). All the tables use the MyISAM engine.

A.1 Scanning lidars

Each scanning lidar setup has a low-level database which contains four tables:

- Scenario
- System
- Wind definition
- Wind data

A.1.1 Scenario

The scenario table has the highest level and has a primary key on the column ”scn_id”, which describes the unique scenario that was running at a certain time on a certain system. In this table we can find the scenario name, the start and end time, the pulse length, the Fast-Fourier transform processing size and 3 ID’s that link this table to other tables. The “gsc_id” is a global scanner number, that allows us to link the scenario to a scanner table (this scanner table is not loaded for RUNE). The column “gw_id” stands for global wind id, and links the scenario to a portion of the coordinate definitions and wind data tables. The global system id “gsys_id” column links the scenario to the system table, which contains system data for this scenario.

A.1.2 System

This table contains general information describing the system when a certain scenario was running. It has columns for the time, latitude, longitude, altitude, heading, pitch, roll and temperature of the system.

A.1.3 Wind definition

The wind definition table contains columns with an ID for start and stop, two corresponding times, the azimuthal angle, the elevation angle, the number of range gates and the accumulation time.

A.1.4 Wind data

The wind data table contains the measured wind data for each range gate. It has columns for the distance of the range gate in decimeter, radial wind speed, CNR and dispersion. The number of rows in the wind data table that is linked to one row in the wind definition table is equal to the amount of range gates.

A.2 Sector-scan setup

The high-level database for the sector-scan measurements, contains one reconstructed table for each averaging period (10 and 30 min and 1 hour). The X, Y and Z coordinates of all range gates are given in “sectorscan_coordinates”. The X and Y are coordinates relative to Vara’s position, while Z is the height amsl. The time is given in GMT. Each time interval contains samples from the time stamp until a certain number of minutes later, i.e. the 10-min averaged data from 00:00 contains samples between 00:00 and 00:10 GMT.

A.3 Dual setup

The dual setup has a similar structure as the sector scan setup, but has two coordinate tables, "dualdoppler_coordinates_1" and "dualdoppler_coordinates_2". This is because of the re-allocation of the range gate positions (Sect. 4.2.2). Each of these tables is linked by an "id" column to tables with the reconstructed wind speeds in 10, 30 and 60 min periods, "dualdoppler_10min_uv_1", "dualdoppler_30min_uv_1", etc. These tables contain the u and v components of the wind speed and the availability for Sterenn and Koshava ("avail_s" and "avail_k"). The coordinate system is also defined relative to Vara and Z is relative to the mean sea level height. The availability is defined as the number of samples which fulfilled the CNR limits (Sect. 4.2.2) divided by the total number of samples in each averaging interval. The time is given in GMT. The time stamps are generated in the same manner as the sector-scan setup.

A.4 Virtual mast setup

The virtual mast setup is composed of a coordinate table and a 10-min mean table: "virtualmast_coordinates" and "virtualmast_10min_uv". The structure in these tables is identical to the dual setup. The time is given in GMT.

A.5 Vertically profiling lidars

Each vertically profiling lidar has four tables associated with it. "windcube_unitxxx_setup" contains the configuration settings, such as sampling frequency, Fast-Fourier window etc., where xxx denotes an identifier for a certain system (see Table 1). It is connected with the "windcube_unitxxx_rundef" table by the column "Setup_idx". This "rundef" table contains, among other things, the sampling interval and the temperature. The table "windcube_unitxxx_fast" contains the radial speed and other measured statistics for each LOS and for each azimuthal position. The table "windcube_unitxxx_10min" contains reconstructed wind speed and direction based on the fast data for every 10-minute interval. The height of the range gates from each system are defined relative to the position of the instrument. Contrary to the scanning lidars, the time is given in GMT. Note that the Høvsøre meteorological mast data are given in GMT+1.

References

Badger, J., Frank, H., Hahmann, A. N., and Giebel, G. (2014). Wind-Climate Estimation Based on Mesoscale and Microscale Modeling: Statistical-Dynamical Downscaling for Wind Energy Applications. *Journal of Applied Meteorology and Climatology*, 53(8):1901–1919.

Berg, J., Vasiljevic, N., Kelly, M., Lea, G., and Courtney, M. (2015). Addressing spatial variability of surface-layer wind with long-range WindScanners. *Journal of Atmospheric and Oceanic Technology*, 32(3):518–527.

Courtney, M. and Simon, E. (2016). Deploying scanning lidars at coastal sites. Technical report, DTU Wind Energy, Roskilde, Denmark.

EEA (2016). http://www.eea.europa.eu/data-and-maps/data/corine-land-cover-2006-raster-3#tab-metadata.

Fairall, C. W., Bradley, E. F., Hare, J. E., Grachev, A. A., and Edson, J. B. (2003). Bulk Parameterization of Air-Sea Fluxes: Updates and Verification for the COARE Algorithm. *Journal of Climate*, 16(4):571–591.

Floors, R., Vincent, C. L., Gryning, S.-E., Peña, A., and Batchvarova, E. (2013). The Wind Profile in the Coastal Boundary Layer: Wind Lidar Measurements and Numerical Modelling. *Boundary-Layer Meteorol.*, 147(3):469–491.

Frank, H. P., Rathmann, O., Mortensen, N. G., and Landberg, L. (2001). *The numerical wind atlas - the KAMM/WAsP method*. Risø-R-1252, Roskilde, Denmark.

Geostyrelsen (2016). http://download.kortforsyningen.dk/content/dhm-2007overflade-16-m-grid.

Gottschall, J. (2016). Floating lidar measurement within RUNE project. Technical report, Fraunhofer Institute for Wind Energy and Energy System Technology, Bremerhaven.

Gottschall, J. and Courtney, M. (2010). Verification test for three WindCube WLS7 LiDARs at the Høvsøre test site. Technical Report Risø-R-1732(EN), DTU, Roskilde, Denmark.

Gottschall, J., Courtney, M. S., Wagner, R., Jørgensen, H. E., and Antoniou, I. (2012). Lidar profilers in the context of wind energy-a verification procedure for traceable measurements. *Wind Energy*, 15(1):147–159.

Gottschall, J., Wolken-Möhlmann, G., Viergutz, T., and Lange, B. (2014). Results and Conclusions of a Floating-lidar Offshore Test. *Energy Procedia*, 53(C):156–161.

Hasager, C. B., Mouche, A., Badger, M., Bingöl, F., Karagali, I., Driesenaar, T., Stoffelen, A., Peña, A., and Longépé, N. (2015). Offshore wind climatology based on synergetic use of Envisat ASAR, ASCAT and QuikSCAT. *Remote Sensing of Environment*, 156:247–263.

Landberg, L., Myllerup, L., Rathmann, O., Petersen, E. L., Jørgensen, B. H., Badger, J., and Mortensen, N. G. (2003). Wind Resource Estimation - An Overview. *Wind Energy*, 6(3):261–271.

Li, X.-M. and Lehner, S. (2014). Algorithm for Sea Surface Wind Retrieval From TerraSAR-X and TanDEM-X Data. *IEEE Transactions on Geoscience and Remote Sensing*, 52(5):2928–2939.

Liang, X. (2007). An Integrating Velocity–Azimuth Process Single-Doppler Radar Wind Retrieval Method. *Journal of Atmospheric and Oceanic Technology*, 24(4):658–665.

Mouche, A., Hauser, D., Daloze, J.-F., and Guerin, C. (2005). Dual-polarization measurements at C-band over the ocean: results from airborne radar observations and comparison with ENVISAT ASAR data. *IEEE Transactions on Geoscience and Remote Sensing*, 43(4):753–769.

Nunalee, C. G. and Basu, S. (2014). Mesoscale modeling of coastal low-level jets: implications for offshore wind resource estimation. *Wind Energy*, 17(8):1199–1216.

Peña, A., Floors, R., Sathe, A., Gryning, S.-E., Wagner, R., Courtney, M. S., Larsén, X. G., Hahmann, A. N., and Hasager, C. B. (2016). Ten Years of Boundary-Layer and Wind-Power Meteorology at Høvsøre, Denmark. *Boundary-Layer Meteorology*, 158(1):1–26.

Peña, A., Gryning, S.-E., and Floors, R. (2015). Lidar observations of marine boundary-layer winds and heights: a preliminary study. *Meteorologische Zeitschrift*, 24(6):581–589.

Pindea, N., Jorba, O., Jorge, J., and Baldasano (2002). Using NOAA-AVHRR and SPOT-VGT data to estimate surface parameters : application to a mesoscale meteorological model. *1st International Symposium on Recent Advances in Quantitative Remote Sensing*, 1161(June):16–20.

Sanchez, R. B. and Rørbæk, K. (2016). Metocean Buoy Deployment. Technical report, DHI.

Thompson, D., Elfouhaily, T., and Chapron, B. (1998). Polarization ratio for microwave backscattering from the ocean surface at low to moderate incidence angles. In *IGARSS '98. Sensing and Managing the Environment. 1998 IEEE International Geoscience and Remote Sensing. Symposium Proceedings. (Cat. No.98CH36174)*, volume 3, pages 1671–1673. IEEE.

Vasiljević, N. (2014). *A time-space synchronization of coherent Doppler scanning lidars for 3D measurements of wind fields*. Phd-thesis, Danish Technical University.

Vincent, C. L., Badger, J., Hahmann, A. N., and Kelly, M. C. (2013). The response of mesoscale models to changes in surface roughness. *EGU General Assembly Conference Abstracts*, 15(10).

DTU Wind Energy
Technical University of Denmark

Frederiksborgvej 399
4000 Roskilde
Denmark
Phone +45 4677 5024

www.vindenergi.dtu.dk